JOURNAL OF THERMOPHYSICS AND HEAT TRANSFER
Vol. 24, No. 3, July–September 2010

Transient Momentum and Enthalpy Transfer in Packed Beds at High Reynolds Numbers

R. Srinivasan*
Defense Research and Development Organization, Hyderabad-500 058, India
and
B. N. Raghunandan†
Indian Institute of Science, Bangalore 560 012, India

DOI: 10.2514/1.39409

An experimental study for transient temperature response and pressure drop in a randomly packed bed at high Reynolds numbers is presented. The packed bed is used as a compact heat exchanger along with a solid-propellant gas generator, to generate room-temperature gases for use in control actuation, air bottle pressurization, etc. Packed beds of lengths 200 and 300 mm were characterized for packing-sphere-based Reynolds numbers ranging from 0.8×10^4 to 8.5×10^4. The solid packing used in the bed consisted of Ø9.5 mm steel spheres. The bed-to-particle diameter ratio was ∼9.5, with the average packed-bed porosity around 0.43. The inlet flow temperature was unsteady and a mesh of spheres was used at either end to eliminate flow entrance and exit effects. Gas temperature and pressure were measured at the entry, exit, and at three axial locations along centerline in the packed beds. The solid packing temperature was measured at three axial locations in the packed bed. A correlation based on the ratio of pressure drop and inlet-flow momentum (Euler number) exhibited an asymptotically decreasing trend with increasing Reynolds number. Axial conduction across the packed bed was found to be negligible in the investigated Reynolds number range. The enthalpy absorption rate to solid packing from hot gases is plotted as a function of a nondimensional time constant for different Reynolds numbers. A longer packed bed had high enthalpy absorption rate at Reynolds number $\sim 10^4$, which decreased at Reynolds number $\sim 10^5$. The enthalpy absorption plots can be used for estimating enthalpy drop across packed bed with different material, but for a geometrically similar packing.

Nomenclature

A	=	inlet area of packed bed
C_d	=	discharge coefficient
C_p	=	specific heat
C_f	=	friction coefficient
D	=	test section internal diameter
Eu	=	Euler number, $\Delta p/\rho_g u_g^2$
$Øp$	=	diameter of sphere used in packing
F	=	force causing flow-momentum loss across packed bed
Fo_d	=	Fourier number based on packing-sphere diameter, $4\alpha_s t/Øp$
G_o	=	mass flux upstream of packed bed
K_e	=	effective thermal conductivity
L	=	packed-bed length
$\dot{m}$	=	mass flow rate
P	=	pressure
ΔP	=	pressure drop
Re_D	=	Reynolds number based on pipe diameter
Re_d	=	Reynolds number based on packing-sphere diameter, $G_o\Phi_p/\mu$
Re_s	=	Reynolds number based on solid fraction, $G_o\Phi_p/\mu(1-\epsilon)$
T	=	temperature
t	=	time
t^*	=	conduction time scale
u	=	velocity
x	=	axial dimension

Subscripts

g	=	gas
i, e, h	=	inlet, exit, and heater stations, respectively
o	=	stagnation condition
s	=	solid
1, 2, 3	=	axial locations along packed bed

Greek Symbols

α	=	thermal diffusivity
ϵ	=	void fraction
Φ	=	energy-absorption ratio
μ	=	dynamic viscosity
η	=	energy-balance ratio
ρ	=	density

Received 27 June 2008; revision received 31 December 2009; accepted for publication 9 January 2010.

*Scientist, Solid Propulsion Division, Advanced Systems Laboratory.
†Professor, Department of Aerospace Engineering.

I. Introduction

PRESSURIZED systems using high-pressure air find many applications such as cold-gas reaction, feed systems in liquid-propellant rocket engines, turbo alternators, etc. The prevailing pressurization methodology uses air-charging units or precharged air bottles. The use of air-charging units downgrades operational readiness, and precharged air bottles are prone to leaks during prolonged storage and pose a safety hazard. Solid-propellant-based gas-generation systems are attractive for such situations, and are advantageous due to compactness and low weight as compared with air bottles. The major requirement is that the exit-gas temperatures should be low enough so as not to thermally affect the components operating downstream. Solid propellants with low flame temperature of around 800 K, which produce inert gases as products of decomposition, are employed in such applications. These decomposition gases are cooled in the packed bed to ambient temperature before entering the pressurizing unit. A typical application is a 6-liter (6×10^{-3} m^3) air bottle pressurized to 35 Mpa in 5 s used in a pressure-fed liquid rocket engine. For a 90 mm diam packed-bed heat exchanger with Ø9.5 mm spheres, the packing-sphere-based

Reynolds number Re_d is $\sim 4 \times 10^4$. During the propellant burn time, the flow between the combustion chamber and packed-bed installation is choked to ensure that packed-bed flow conditions do not affect the combustion process. After pressure equalization between the gas generator and pressurized unit, the gas is stagnant. No further energy transfer occurs, and, in effect, the stored heat in the solid packing of the bed is unused.

A schematic representation of the gas generator with the heat exchanger is shown in Fig. 1.

Solid-propellant formulations generally contain additives for stable propellant combustion, long shelf life, and mechanical properties, which sometimes do not combust completely and exit along with condensed-phase species from the nozzle. Although the products of combustion contain these solid-phase species (5 to 10 μ in size), studies have shown that their mass fraction is low (<7%). Therefore, the inlet flow may be treated as a single-phase system for the purpose of pressure-drop and heat-transfer characterization. The packed bed encounters a steady mass flow rate but with a varying inlet temperature. The objective of the present work is to obtain pressure and enthalpy-drop correlations for randomly packed beds up to $Re_d \sim 8 \times 10^4$.

II. Background Literature

Fluid-flow and heat-transfer phenomena in randomly packed beds have received much attention due to a number of practical applications. These applications include pebble-bed heaters, thermal-energy storage systems, compact heat exchangers and catalytic reactors. The physical processes in packed beds have been modeled by both theoretical and experimental approaches. Beasley and Clark [1] have experimentally studied transient response of packed beds in Reynolds number range of 90 to 660, while Gunn and De Souza [2] have suggested a Nusselt number correlation up to a Reynolds number of 8.5×10^3. Many investigations on heat transfer have been in the Reynolds number ranges of around 1×10^4. A summary of experiments conducted by different investigators with details such as inlet-flow conditions, Reynolds number range, packing-material shape and size, etc., have been tabulated by Wakao et al. [3]. As per their tabulated summary, the maximum Reynolds number of the experimental investigations (by Lindauer) was 1.82×10^4. Vilemas et al. [4] have carried out experimental heat-transfer studies on a two-layer fixed bed of spheres welded between two perforated plates up to Reynolds number of 1.5×10^4. A useful result from their study is that a decreasing perforation-diameter-to-sphere-diameter ratio increases the heat transfer in the initial layers of spheres. This entry effect is eliminated in the present study by use of a Ø9.5 mm-sphere mesh. The sphere mesh is a replacement for commonly used wire meshes or perforated plates holding the bed of spheres in place.

The text on transport phenomena by Bird et al. [5] lists a number of correlations for pressure drop across packed beds, such as the Ergun and Tallmadge equations. The use of the Tallmadge equation given below,

$$\left(\frac{\Delta P \rho_g}{G_O^2}\right)\left(\frac{\phi_p}{L}\right)\left(\frac{\epsilon^3}{1-\epsilon}\right) = 150\left(\frac{1-\epsilon}{\phi_p G_o/\mu}\right) + 4.2\left(\frac{1-\epsilon}{\phi_p G_o/\mu}\right)^{1/6}$$

is often recommended for $Re_s = \Ø_p G_o/\mu(1-\epsilon) < 10^5$. The pressure drop calculated from the correlation had a rather low value when compared with pressure drop obtained in one of the present experiments. Table 1 gives the values for pressure drop (expressed in Euler number) obtained from the experiment and from the Tallmadge correlation.

The reason probably is due to wall effects of a finite packing. Experimental results of different researchers are contradictory [6]; some report an increase in pressure drop, and others report a reduction in pressure drop with reference to an infinite bed. The pressure drop is an important parameter that influences the upstream pressure of the packed bed, which in practical applications determines the combustor pressure required in the solid-propellant gas generator to maintain choked flow.

Gauvin and Katta [7] have studied packed-bed flow with solid and hollow particles using a correlation for apparent bed porosity in Reynolds number range of 400 to 0.28×10^4. They have indicated an apparent reduction in flow area with increasing Reynolds number as a result of vortices in the interstitial spaces. Glaser and Thodos [8] used an electrically heated packed bed with cold flow passing through packings of spheres, cubes, and cylinders of different sizes to study heat transfer under steady-state conditions. Thermocouples were attached to particle surfaces for temperature measurement of solid packing. Thermocouples placed in the void spaces measured the gas temperature. The steady-state Colburn heat-transfer factors were evaluated for Reynolds number up to 1×10^4. The heat-transfer factors could not be correlated for different sizes of the same geometric shape, particularly at low Reynolds numbers, and were attributed to a ratio of particle-size-to-packed-bed diameter. The schemes of experimental investigations devised by different investigators have served as a valuable input for the design and configuration of the present experimental setup.

Attempts to correlate temperature and pressure-drop data in order to simplify the estimation of enthalpy drop from drag data have been attempted. Glaser and Thodos [8] have indicated that such a correlation was unlikely until the contributions of skin friction and profile drag are estimated. However, Fukuda et al. [9] have reported a correlation between pressure drop and heat transfer valid up to Reynolds number of 10^3. At Reynolds numbers $\sim 4 \times 10^4$, profile-drag contribution to pressure drop can be significant due to wake interactions in successive sphere layers. Hence, the present investigation included study of both pressure and enthalpy drop across the packed bed.

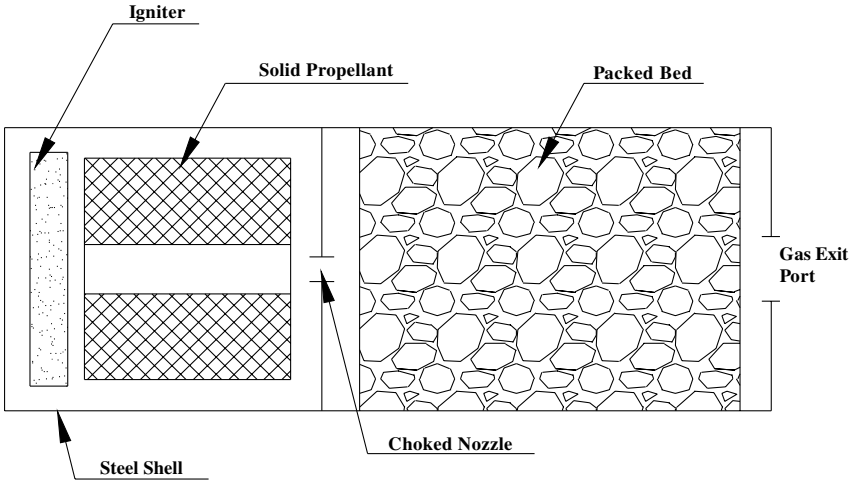

Fig. 1 Sketch of gas generator with heat exchanger.

Table 1 Comparison of pressure drop from experiment with correlation

Re_s	Euler number	
	Tallmadge correlation	Experimental data
1.73×10^4	124.2	206.9
4.62×10^4	105.1	100.6

A substantial amount of work has been carried out recently, using a numerical approach [10,11] for simulating heat transfer and fluid flow in packed beds. Nijemeisland and Dixon [12] have performed numerical simulations for low tube-to-particle diameters and compared them with experiments in an attempt to describe the local flow and heat-transfer processes. To facilitate a turbulent-flow solution, contact points between particle–particle and particle–wall had to be eliminated in their numerical model. The Reynolds number ranges were 373 to 1922, the limits imposed by their experimental setup. Kuwahara et al. [13] have attempted a numerical experiment using a single structural unit for determining heat-transfer coefficient without any empiricism. Their study is in the Reynolds numbers range of 1 to 100. The single-structural-unit model may not capture the flow complexities for successive layers downstream, as the flow is not self-similar. The change of boundary-layer attachment points due to effects of turbulence and pressure gradients in subsequent sphere layers results in a very complex flow, as reported by Van Der Merwe and Gauvin [14].

Modeling complexities of random packing, uncertainties in flow profiles, turbulence levels, and, more importantly, the nonavailability of data at high Reynolds number ranges for validation render this problem less amenable for a numerical solution. The feasibility of rigging an experimental setup that could simulate the Reynolds number range and randomness of packing with required instrumentation also contributed to the choice of experimental route. It was felt that the experimental study could add to the database on packed-bed pressure drop and heat transfer, particularly at $Re_d \sim 10^4$.

III. Experimental Facility

Design and analysis of the packed-bed heat exchanger requires knowledge of time-dependent convective-heat-transfer characteristics between porous-matrix and hot-gas flow. The porous matrix consists of tight packing of steel spheres in between steel meshes. For the present simulation, initially, an electric-heating-based system was considered for supply of hot air to the packed bed. The power requirements for mass flow rate of 1 kg/s and temperature difference of about 200°C worked out to be 200 kW. Because of the high power requirement, the electric-heater system was ruled out, and a hydrogen–air-heater-based system was adapted. Gas temperatures of order of 150 to 200°C may be obtained by combustion of a few grams of hydrogen, and connected-pipe mode tests can be carried out by interfacing the packed bed to the hydrogen–air combustor device.

A dedicated experimental facility was designed ab initio and built for the present work. The experiments were planned in an open-loop setup containing an air compressor, air-storage bottle, hydrogen–air combustor, settling chamber, orifice meter, packed-bed test section, and data-acquisition system. A schematic diagram of the experimental test facility is shown in Fig. 2. The air from the compressor is dried and filtered before being filled in the storage bottle. The fuel line consists of a bank of hydrogen and nitrogen cylinders. Nitrogen gas was used for purging the test section after the hot test. The pressure setting downstream of the air bottle and hydrogen cylinders was controlled by using dome pressure regulators. Electromechanical actuators were used to operate the airflow and hydrogen-flow lines remotely from a control room. The ignition of hydrogen–air mixture was by pyro cartridges, and flame holding was achieved by creation of a recirculation zone with a *V* gutter in the combustor.

The operation of the hydrogen–air combustor was at design conditions with respect to the air-to-fuel ratio that enabled ignition, flame stabilization, and stable combustion. Since the packed-bed test section required different mass flow rates, a bypass vent (see Fig. 2) connected before the test section diverted the excess flow. The test-section exit was closed (see Fig. 3) with a plate having multiple orifices that could be blanked with grub screws. Since the flow through the exit orifices was choked, the downstream atmospheric effects on flow in the test section were absent.

The flow measurement to the test section was made by using an orifice plate. The orifice-plate manufacture, installation procedure, and tolerance were as per international standard [15]. Four orifice plates of sizes 25, 20, 15, and 12.5 mm were fabricated for different flow rates. Orifice plates were selected corresponding to the flow rate to ensure subsonic flow and recordable pressure drop across the orifice. The pressure drop was measured by means of a differential pressure transducer.

The test-section pipe hardware and flanges were fabricated using structural steel as per industrial standard. The test section had an internal diameter of 90 mm, and the maximum packed-bed length that could be accommodated was 500 mm. The test section had provision for adjustable inserts to vary packed-bed length from 100 to 500 mm in steps of 100 mm. The solid packing in the test section consisted of commercially available Ø9.5 mm carbon-steel ball bearings. The packing was held on both sides of the test section by a

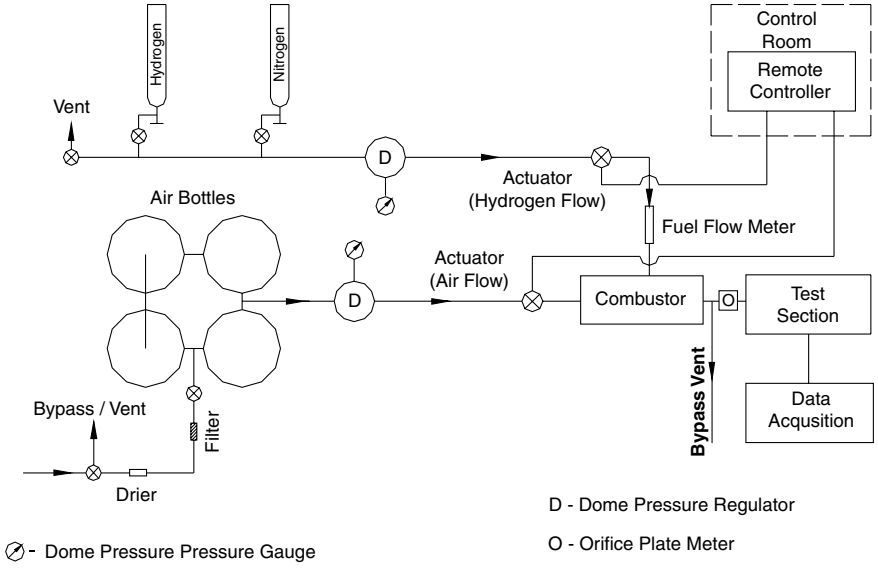

Fig. 2 Schematic representation of test facility.

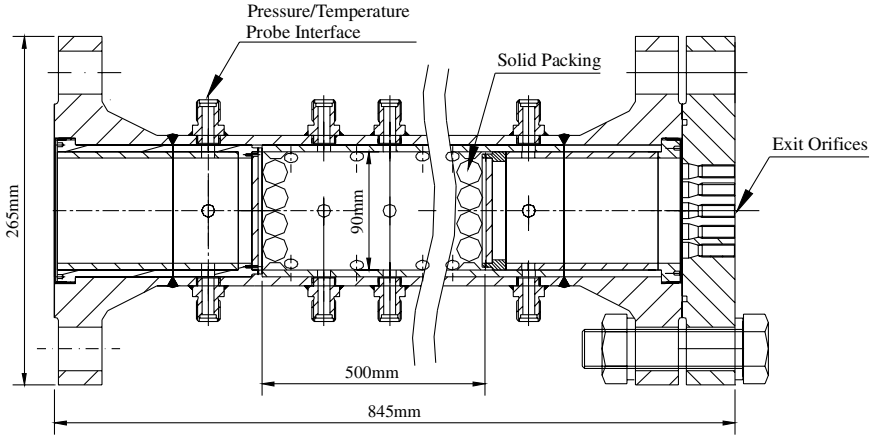

Fig. 3 Sketch of test section.

mesh of Ø9.5 mm steel spheres, which was made by stringing the steel spheres on Ø1 mm rods, and the rods were subsequently mounted on rings (see Fig. 4). The mesh was part of the packed bed and was included in the packed-bed length. The water in the flower vase indicates the direction of the gravity vector and that the spheres are rigidly held, thus eliminating the possibility of nonuniform porosity.

The packing of steel spheres was laid up layer by layer, and the setup was vibrated to ensure packing uniformity. Industrial-grade sealant applied to retainer rings held the solid packing in place and prevented loosening during handling and testing. Compression-molded silica phenolic (silica cloth with phenolic resin) of 5 mm thickness was provided along the test-section walls to avoid radial heat transfer to the test section. The insulation also eliminated longitudinal heat conduction along test-section walls. A stainless-steel mesh of 1 mm spacing between wires was provided at an upstream location, eight diameters away from the test section, to damp out eddies and flow disturbances introduced by the connecting pipe to the test section.

K-type thermocouples were used for measuring the gas temperature and solid-phase temperature inside the packed bed at different locations. The thermocouple unit consisted of a mineral-insulated sheath with a leak-proof installation housing at one end. The diameter of the sheath was 1.6 mm, and the conductor diameter was 0.23 mm. The thermocouples had an accuracy of ± 0.5°C in the calibrated temperature range of 35 to 200°C.

The gas temperature at different axial locations was measured by a fused junction in insulated sleeve housing to avoid contact with solid packing. The insulated sleeve had passages for gas flow, and the passages were oriented towards the gas flow during the packed-bed assembly. The thermal discontinuity between the fused junction and steel packing was ensured by an *electrically open* check, between the solid packing and each of thermocouple leads, before each test run. The maximum-value-of-time constant, as evaluated upstream of the packed bed by an empirical relation [16] using mass velocity (at lowest investigated Reynolds number range $\sim 10^4$) and average inlet gas temperature, was of the order of 0.4 s.

Fig. 4 Entry and exit mesh of steel spheres.

The solid-packing temperature was measured by positioning the fused thermocouple bead at the sphere center thorough a suitably drilled hole by means of a fixture. The bottom opening was closed by fastening a screw dipped in two-component epoxy resin that ensured leak-proof locking. The thermocouple bead was kept in thermal contact with the steel sphere by filling the drilled hole with mercury. An electrical continuity check was done between the surface of the steel sphere and individual thermocouple leads, to ensure thermal contact through the filled mercury. To retain the filled mercury, the top opening of the sphere was sealed by two-component epoxy resin. The epoxy resin cured at room temperature and had sufficient thermal serviceability to seal the mercury in the cavity for test temperatures of 200°C. For both types of thermocouple installation, the sheath lengths were chosen so as to locate the insulated-sleeve housing (for gas temperature) and the steel-sphere housing (for solid-packing temperature), along the centerline of the packed bed. The installation scheme with photographs of the thermocouples for solid-packing temperature and gas-temperature measurement are shown in Figs. 5 and 6. The change in thermal capacity of the sphere due to mercury was less than 10%. The Biot number evaluated from packed-bed heat-transfer data of Glaser and Thodos [8] was ~ 0.11 (Reynolds number $\sim 10^4$), enabling a lumped mass assumption for the steel sphere with thermocouple.

Three gas-temperature thermocouples were located as shown in Fig. 7 to study the temperature distribution at the test-section entry. The temperatures at locations A, B, and C for one of the experimental runs were 82.5, 81.8, and 80.4°C, respectively. The variation in temperature measured at the three locations was $\sim 2.5\%$, validating the assumption of constant inlet temperature at the cross-section.

The pressure transducers were of strain-gauge type with an accuracy of $\pm 1\%$ of full-scale output and were balanced by a Wheat stone bridge. The maximum transducer-pressure rating chosen was 50% higher than the maximum expected pressure in a test. A 64-channel data-acquisition system with 1 KHz sampling rate was used, and all tests were conducted at ambient temperature (27 to 40°C).

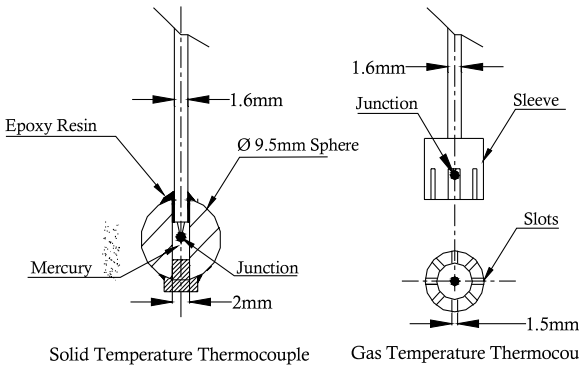

Fig. 5 Installation scheme for solid- and gas-temperature thermocouples.

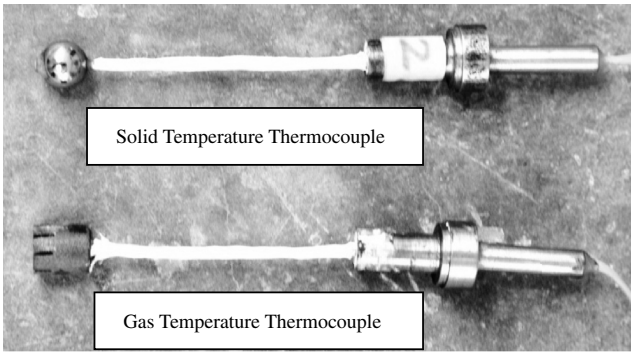

Fig. 6 Solid and gas thermocouples after installation.

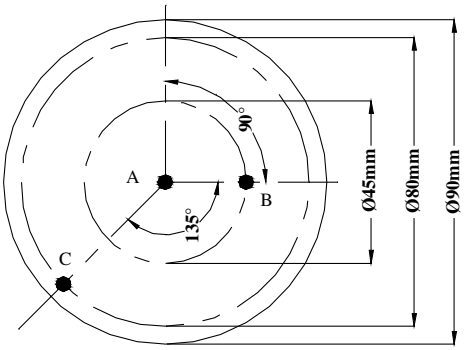

Fig. 7 Thermocouple locations for estimation of cross-sectional temperature variation.

IV. Experimental Procedure

The combustion chamber of the solid-propellant gas generator is uninsulated, which results in heat loss from combustion gases to the walls. This leads to a varying outlet-gas temperature from the combustion chamber. Therefore, the experimental condition for the present investigation is steady mass flow rate with varying inlet temperature, which approximates the operation of the heat exchanger for characterization of pressure and enthalpy drop at discrete Reynolds numbers. During the static tests, the airflow was allowed to stabilize, for which the time scale was of the order of 5 s. The hydrogen-fuel injection commenced 6 s after airflow start, with the pyro-cartridge ignition 11 s after start of airflow. Upstream pressure and exit-orifice area for the required flow rates were estimated by solution of one-dimensional-mass-continuity and momentum-conservation equations. The flow resistance in the test section due to solid packing was initially approximated by the Tallmadge equation referred to earlier. Later, this upstream pressure had to be increased to obtain the desired mass flow rate during calibration runs. Cold-flow calibration for pressure regulator (fuel) was done by passing nitrogen gas in the fuel line to estimate the hydrogen flow rate for the required temperature in the combustor. A number of calibration runs were conducted to establish the upstream pressure settings, downstream orifice opening, and fuel-line-injection pressure setting. During the hot static test, hydrogen replaced the nitrogen gas in the fuel line. Since the flow rate of hydrogen in the combustor was low ($\sim$0.15%), the chemical composition of air at combustor exit was assumed as unaltered.

Pressure drop and enthalpy drop across randomly packed beds consisting of Φ9.5 mm spheres were studied for cold and hot inlet flows separately. The ratio of test-section diameter to sphere diameter was $\sim$9.5. The values of density, specific heat, and thermal conductivity for the solid-packing material (carbon steel) are 7850 $\mathrm{Kg/m^3}$, 500 J/Kg K, and 52 W/mK respectively. The internal diameter of the test section was 90 mm, and packed-bed lengths of $\sim$200 and $\sim$300 mm were studied. The test-section volume was computed by measuring the internal diameter at five locations, selected randomly, and the postassembly packed-bed length. Bed porosity was calculated from the weight of the spheres and the test-section volume. A schematic representation of the instrumentation plan is shown in Fig. 8. Gas temperature, static, and stagnation pressure were measured at entry and exit of the test section.

Static pressure, gas temperature, and solid-packing temperature were measured along the packed-bed axis at lengths of 50, 100, and 150 mm (packed-bed length $\sim$200 mm) and 75, 150, and 225 mm (packed-bed length $\sim$300 mm). The description of solid packing, bed lengths, and other experimental conditions are summarized in Table 2.

Figure 9 shows a plot of Reynolds number (as computed online by the data-processing unit) vs time for a typical experimental run (packed-bed length 313 mm). The total time of observation and data logging for this experimental run was $\sim$35 s. Variation in Reynolds number $\sim$4.3% toward end of the experimental run was observed after the initial flow stabilization and ignition transient.

The variations were due to an increase of dynamic viscosity ($\sim$10% for temperature variation from 35 to 121°C) and the operational characteristics of the pressure regulator. The first peak corresponds to onset of cold flow, and the second peak corresponds to ignition of the hydrogen–air mixture. Figure 10 shows the stagnation pressure at the entry and exit of the packed bed: the average stagnation pressure drop is $\sim$0.027 Mpa (see Fig. 11). From Table 2 it can be observed that the maximum inlet velocity to the packed bed is $\sim$12.7 m/s, which can increase to $\sim$28.9 m/s inside the packed bed for $\epsilon = 0.44$. The flow Mach number inside the packed bed is $\sim$0.067, and, as such, the flow is incompressible.

Figures 12 and 13 show gas-phase and solid-packing temperature variation with time, respectively, for a packed-bed (length 215.5 mm) experimental run. An initial temperature peak at $\sim$2.5 s can be observed in the gas temperatures (T_{g1}, T_{g2}, and T_{g3}) due to hot gases emanating from pyro-cartridge firing before ignition of hydrogen fuel. The solid-packing temperatures (T_{s1}, T_{s2}, and T_{s3}) indicate a minor temperature rise (due to hot pyro-cartridge gases) because of thermal inertia. The gas temperature drops axially along the packed bed at any time instant. The exit-gas temperature T_e increases with time as the temperature difference between gas and solid packing diminishes. Verification for energy balance across the packed bed was done by selecting a control volume (see Fig. 8) containing the

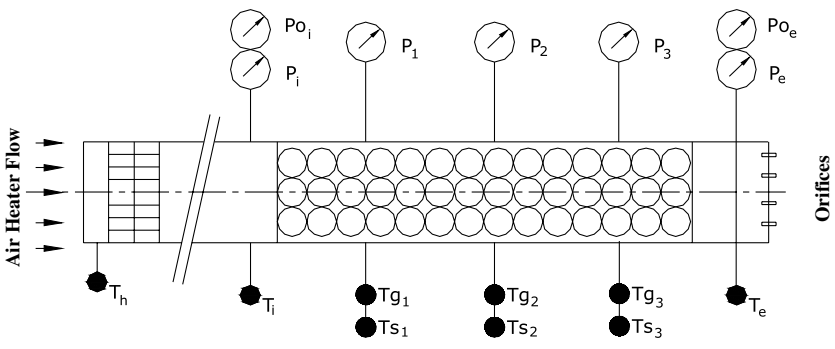

Fig. 8 Instrumentation plan for packed-bed test section.

Table 2 Experimental conditions for packed-bed test runs

Packed-bedlength L (mm)	Void fraction ϵ	Maximum inlet-flow temperature T_i (°C)	Inlet-flow velocity u_g (m/s)	Re_d (cold flow and hot flow)
		37.2	3.2	$\sim 1 \times 10^4$
		73.4	3.6	$\sim 1.1 \times 10^4$
		35	4.3	$\sim 2.6 \times 10^4$
215.5	0.44	73.6	4.9	$\sim 2.7 \times 10^4$
		38	7.4	$\sim 4.9 \times 10^4$
		83.5	9.2	$\sim 4.6 \times 10^4$
		37.5	9.1	$\sim 7.8 \times 10^4$
		163.1	12.7	$\sim 6.5 \times 10^4$
		30.1	2.3	$\sim 0.8 \times 10^4$
		121	2.1	$\sim 1 \times 10^4$
		29	4.2	$\sim 2.5 \times 10^4$
313	0.42	81.5	4.8	$\sim 2.7 \times 10^4$
		28	8.0	$\sim 5.1 \times 10^4$
		165.8	10.2	$\sim 4.4 \times 10^4$
		28	8.4	$\sim 7.4 \times 10^4$
		92.2	12.1	$\sim 8.5 \times 10^4$

gas temperature (T_{g1} and T_{g3}) and solid-packing temperature (T_{s1} and T_{s3}) thermocouples. The integrated enthalpy change of solid packing at time t is compared with the summation of inlet-flow enthalpy from time $t = 0$ to t, as

$$\eta = \frac{A(1-\epsilon)Cp_s\rho_s \int_0^L T_s(x)\,\mathrm{d}x}{\sum_0^t \dot{m}_i\, Cp_g(Tg_1 - Tg_3)\Delta t}$$

The energy-balance ratio η worked out to be $\sim$0.94. The thermal losses were to the test-section walls, thermocouple sheaths, and thermocouple housings.

V. Treatment of Data

Around 30 tests were conducted for calibration runs and different static test combinations as shown in Table 2. The calibration runs were for estimating the dome pressure settings for the required mass flow rate of air and, hence, Re_d through the packed bed. Experimental reproducibility of mass flow rate was verified during the calibration runs conducted for hydrogen-fuel injection pressure, which used the same dome pressure settings as those obtained for cold-flow tests. Computation of mass flow rate through the packed-bed test section was from pressure differential across the orifice-plate meter. Using a third-degree curve fit for C_d with Reynolds number as dependent variable (from tabulated data for orifice plates with flange tapping), an initial value for C_d was estimated. The mass flow rate was calculated, and Re_D, pipe-diameter-based Reynolds number (function of mass flow rate), and C_d (function of Re_D) were updated. The values for Re_D, C_d, and mass flow rate converged after a few iterations. The temperature effect on gas viscosity at packed-bed inlet was accounted for using reduced viscosity vs reduced temperature plots [5]. The measurement error [15] in the mass flow rate of the orifice-plate meter was $\pm 0.6\%$. The packing-sphere-based Reynolds number was calculated from the mass flux. After evaluation of Reynolds number obtained in the tests, those tests in the desired Reynolds number ranges were sorted separately for further analysis. Axial-flow velocity in the packed-bed axis was computed from the mass-conservation equation, using density values as obtained from static pressure measurements along the test-section walls.

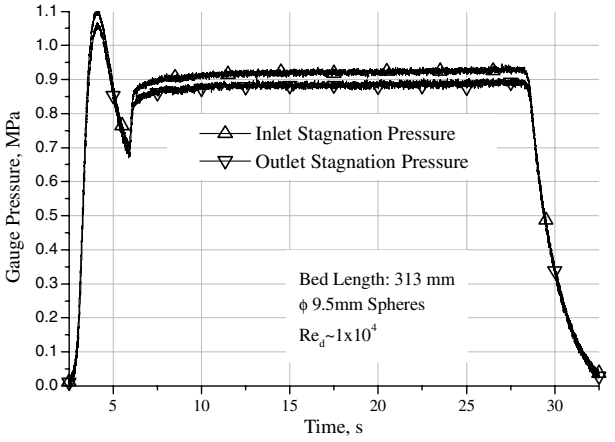

Fig. 10 Plot of inlet and outlet stagnation pressures.

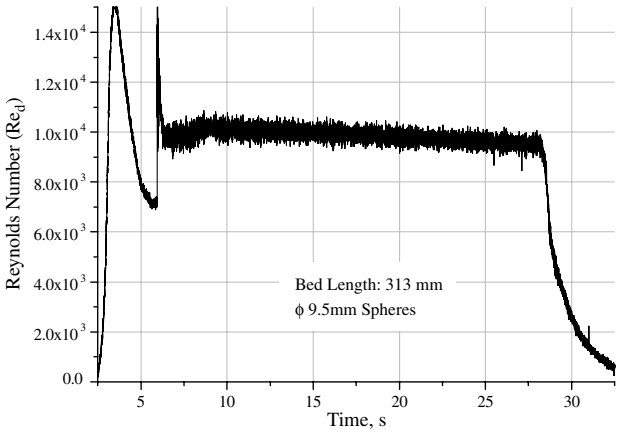

Fig. 9 Plot of Reynolds number with time for hot-gas flow.

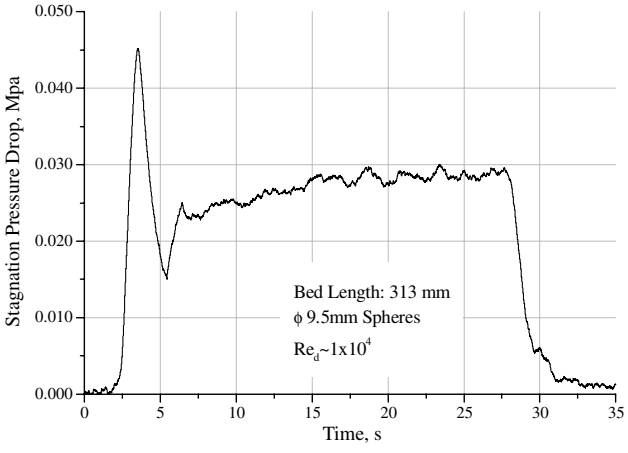

Fig. 11 Plot of stagnation pressure drop.

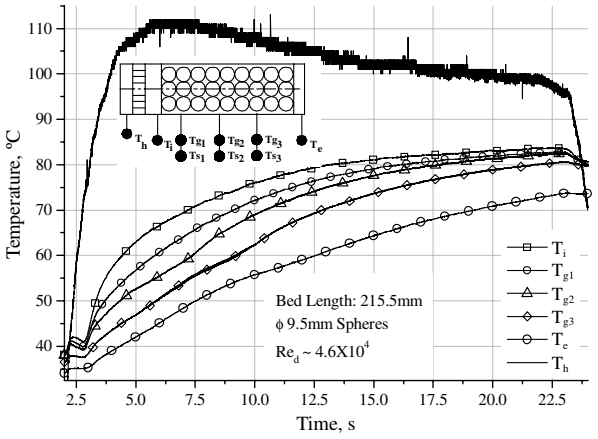

Fig. 12 Plot of gas-temperature variation across packed bed with time.

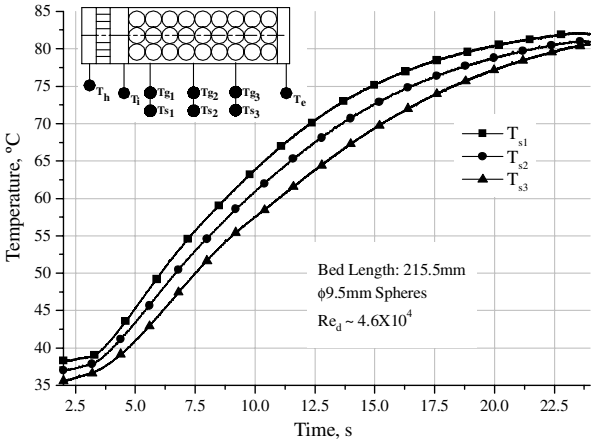

Fig. 13 Plot of solid-packing temperature variation across packed bed with time.

VI. Data Correlation and Results

The flow inside a packed bed corresponds to some degree of flow in channels with alternating expansion and contraction. The freestream turbulence effect is only in the first two layers of spheres, and grid effect of upstream sphere layers generates a turbulence pattern of its own. The presence of upstream rows of spheres in the packed bed results in the flow to the inner row being vortical with nonuniform velocity distribution, and turbulence generation in space between the spheres is a function of Reynolds number and pore space. Investigations on flow regimes in packed beds using microelectrodes by Latifi et al. [17] have indicated the Reynolds number for transition (unsteady-state laminar) as $110 < Re_d < 370$. Jolls and Hanratty [18] in their visual study of motion of colored plume of fluid in dumped bed of spheres also have suggested transition to turbulent flow at $Re_d \sim 300$. The present investigation at $Re_d \sim 10^4$ is therefore in the turbulent-flow regime. The upstream pressure accelerates the flow through the packed bed. However, irreversible losses due to eddies, wakes, and flow in interstices of the packed bed decreases the momentum of the flow. A pressure gradient is required to maintain the flow across the packed bed. The variables influencing the resistance that changes the flow momentum are identified as [19]

$$F = F(\rho_g, u_g, x, \mu, P, \phi_p)$$

In the above functional relation, pressure P and flow density ρ_g are related. Dimensional analysis of variables leads to three independent groups. The nondimensional groupings are Euler number ($\Delta P/\rho_g u_g^2$), Reynolds number ($G_o \emptyset_p/\mu$), and friction coefficient ($C_f = F/\rho_g u_g^2 L^2$). The Reynolds number has the packing-sphere diameter as the length scale, with mass flux representing the inertia force, to characterize wake-formation and flow-separation phenomena. The Euler number in the present case represents the pressure drop required to overcome momentum losses in the packed bed. The packed-bed-length scale appears in the friction coefficient C_f.

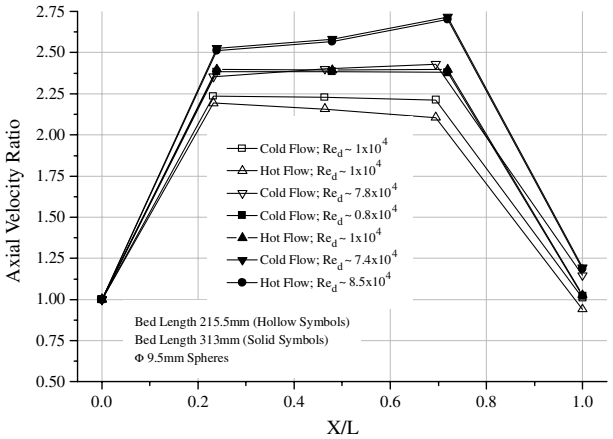

Fig. 14 Plot of velocity ratio along nondimensionalized packed-bed length.

A. Axial-Velocity Profiles

The plots for axial-velocity ratio (made nondimensional with inlet velocity) across nondimensionalized packed-bed length are shown in Fig. 14.

The velocity ratio increases at high Reynolds numbers and with increase in packed-bed length, with an exception in an experimental run of packed-bed length 215.5 mm with hot-gas flow. Since the flow is subsonic, the axial variation in density is negligible, and increase in velocity ratio is due to an apparent decrease in flow area in the packed bed axially. The apparent area variation is due to formation of wakes and boundary-layer interactions within the flow after successive sphere layers. For the experimental condition of cold-gas flow, the flow condition can be considered as a case of Fanno flow, in which subsonic flow accelerates. The case of hot-gas flow can be treated as Rayleigh flow, in which subsonic flow decelerates due to cooling as the gases transfer their enthalpy to the solid packing. Flow deceleration because of cooling is observed to be dominant over acceleration due to friction in the case of 215.5 mm packed bed with Ø 9.5 mm packing ($Re_d \sim 1 \times 10^4$) leading to a decrease in velocity ratio.

B. Pressure-Drop Correlations

Initial cold-flow experiments of packed bed of 215.5 mm length consisting of Ø 9.5 mm spheres with porosity ~0.44 indicated pressure drops ~67% higher at $Re_s \sim 1.73 \times 10^4$ ($Re_d \sim 1 \times 10^4$). The pressure-drop difference between the Tallmadge correlation and experiment seemed to decrease at $Re_s \sim 4.62 \times 10^4$ ($Re_d \sim 2.6 \times 10^4$). The Euler number vs Reynolds number curve fits for cold and hot inlet flows are shown in Fig. 15. Regression analysis was carried out for 95% confidence band, and the correlation coefficients for 313 and 215.5 mm packed beds were 0.93 and 0.63, respectively. The Euler number reaches asymptotic values at high Reynolds numbers $\sim 8.5 \times 10^4$.

Zukauskas [20], in his study for cross flow over staggered tube bundles, has reported flow with strong longitudinal mixing with turbulence in tube spacing at freestream Reynolds numbers higher than 10^3 ($Re_d \sim 10^2$). The drag of the tube bundles was proportional to the number of tube rows, and the Euler number decreased from Reynolds number $\sim 10^4$ ($Re_d \sim 10^3$) toward Reynolds number $\sim 10^5$ ($Re_d \sim 10^4$). Assuming the packed bed as a three-dimensional analogue of staggered tube bundles, in which the tube spacing tends to a minimum, a similar effect of decrease in drag coefficient (corresponding to pressure drop) with increasing Reynolds number and an increase in pressure drop with packed-bed length effect are

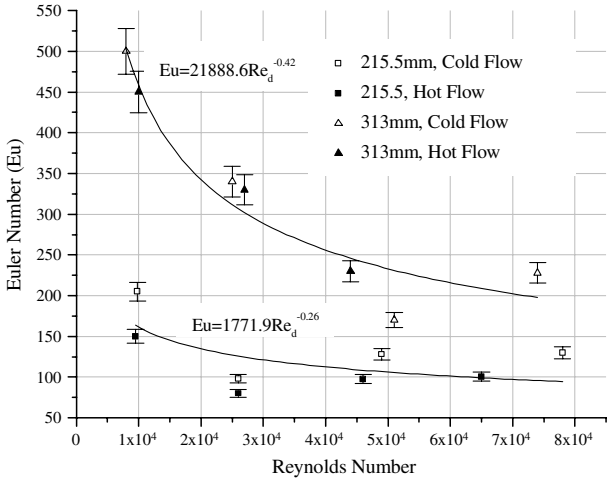

Fig. 15 Plot of Euler number with Reynolds number.

observed in the experiments. Studies by Zukauskas on heat transfer in layers of staggered tube bundles have established that transition occurs from subcritical to critical flow at freestream Reynolds number $\sim 10^5$ ($Re_d \sim 10^4$). Assuming the packed bed as a subset of staggered tube bundles, in which the tube spacing tends to a minimum, a similar phenomenon of decrease in drag coefficient (corresponding to pressure drop) is observed. The effect of flow transition on pressure drop is more apparent in the case of longer bed length.

Table 3 gives the uncertainties in measured variables used to evaluate the Euler number. Combining the uncertainties, in the sense of root mean square, the uncertainty in Euler number at 95% confidence level works out to be 5.6%. Increased porosity near the wall due to radial variation of void fraction causes flow maldistribution that influences the pressure drop. At $10 > D/\emptyset_p > 4$, pressure-drop uncertainties of the order of $\pm 20\%$ are possible [21].

Radial variation of void fraction leads to generation of near-wall bypass flow, which increases with a decrease of tube-to-sphere-diameter ($D/\emptyset_p$) ratio. Thus, while evaluating experiments for pressure-drop correlations, the mean velocity computed from mass flow rate is higher than the actual axial velocity at the packed-bed centerline. For $D/\emptyset_p < 10$, the wall effect is important for streamline or transitional flow conditions, and at high Reynolds numbers the effect of void fraction is dominant [6]. Using the results of Achenbach [22] to account for the effect of bypass flow at $Re_d \sim 10^4$, the pressure drops obtained for $D/\emptyset_p \sim 9.5$ are $\sim 15\%$ lower than for the case of infinitely extended beds ($D/\emptyset_p \to \infty$).

C. Enthalpy Drop

The total transient energy change of the packed bed is due to internal energy change of gas phase and solid packing. However, the heat capacity of the solid packing is three orders of magnitude higher than the gas phase, and, hence, the gas-phase heat capacity can be neglected [23]. Moreover, incoming hot gases, which transfer energy to the solid packing, continuously replace the gas in the void space. The enthalpy drop of the hot-gas flow across the packed bed is a function of axial conduction along the packed bed and internal energy change of solid packing. The viscous dissipation is negligible because of low flow velocities. The ratio of magnitude of convection to diffusion (Peclet number) had an order of magnitude 10^5 for the gas phase at $Re_d \sim 10^4$, which implies that axial conduction through the gas phase is negligible. Therefore, the effective axial thermal conductivity of the solid packing is a function of contact pattern and solid thermal conductivity. Chan and Tien [24] have suggested a correlation for conductance of packed spheres in vacuum that compares satisfactorily for available experimental data. The effective thermal conductivity neglecting any deformation of the sphere packing was 0.27 W/mK for Ø9.5 mm sphere packings from their correlation. The ratio of internal energy change due to axial conduction and total internal energy change gives the order of magnitude of axial conduction across the solid packing. This ratio using solid-packing temperature values measured at axial locations of 50, 100, and 150 mm from an experimental run (see Fig. 12) was of the order of 10^{-5}. Yagi et al. [25], in their study, also have suggested the insignificance of axial thermal conduction at $Re_d > 10^3$, since axial temperature gradients in packed-bed reactors do not occur at high Reynolds numbers. Additionally, the time scale ($t^* = \rho_s c_s L^2/k_e$) for axial conduction across the packed bed is of the order of 10^4, which is three orders of magnitude higher than the flow duration in the packed bed. These conditions indicate that axial conduction across the solid packing is insignificant for $Re_d > 10^4$, as corroborated by the present experimental study.

Table 3 Uncertainty in measured variables

Variable	Uncertainty
ΔP	Uncertainty 1%, based on calibration data
ρ_g	Total uncertainty 1.12%, based on uncertainty in pressure (1%) and temperature (0.5%)
u_g	Total uncertainty 2.7%, based on uncertainty in mass flow rate (2%), temperature (0.5%), pressure (1%), and test-section diameter (0.7%)

The enthalpy absorbed from $t = 0$ to the final time is the difference between the inlet and outlet temperature integrated with time. The energy-absorption ratio ϕ is defined as energy absorbed until the current time step to the total energy absorbed over the entire period:

$$\Phi = \frac{\int_{t1}^{t+\Delta t} \int_{X_1}^{X_2} \rho_g u_g \in C_{p_g} T_g \, \mathrm{d}t}{\int_{t1}^{t2} \int_{X_1}^{X_2} \rho_g u_g \in C_{p_g} T_g \, \mathrm{d}t}$$

Figure 16 shows the energy-absorption ratio as a function of Fourier number for the packed beds. The Fourier number represents conduction resistance of packing material and is indicative of the enthalpy absorbed by the packed bed from the hot-gas flow. A lower-energy absorption rate is observed for 215.5 mm-long packed bed than for 313 mm packed bed at $Re_d \sim 1 \times 10^4$. However, at $Re_d \sim 1 \times 10^5$, the 215.5 mm packed bed has higher energy absorption than the 313 mm packed bed. The higher-energy absorption rate of the 313 mm packed bed at $Re_d \sim 1 \times 10^4$ is not due to larger thermal mass, since the experiments at $Re_d \sim 4.6 \times 10^4$ for 215.5 mm packed-bed length and at $Re_d \sim 4.4 \times 10^4$ for 313 mm packed-bed length indicated a converse result.

Since the axial-conduction effects are negligible, the packed bed can be visualized as a subset of staggered tube bundles for purposes of fluid dynamic analogy and heat transfer. Zukauskas has carried out extensive studies on heat transfer [26] through staggered and inline tube bundles and has documented data from a number of researchers.

In his study, flow turbulization in the initial two rows at freestream Reynolds number range of 10^3 to 10^4 ($Re_d \sim 10^2$ to 10^3) resulted in high heat-transfer coefficients ($\sim 35\%$ higher) from third row onward. A similar type of result is observed here in packed bed of 313 mm length, where higher heat-transfer coefficients at aft end leads to higher energy absorption at $Re_d \sim 10^4$. At Reynolds number $\sim 10^5$ ($Re_d \sim 10^4$), Zukauskas has reported occurrence of supercritical flow with transition from predominantly laminar to mixed flow in staggered tube bundles. The mixed flow had vortices with enhanced turbulence and low flow velocity in recirculation zones. Zukauskas and Poskas [26], in their experimental study of tightly packed staggered bundles, have shown the effect of velocity fluctuations in turbulent flow on heat-transfer coefficient to be an order of magnitude smaller. Lower flow velocities in recirculation zones of the packed bed due to close packing, unlike staggered tube bundles, resulted in lower heat-transfer coefficients at aft end of sphere packing. This resulted in slower energy-absorption rate for 313 mm packed-bed length at $Re_d \sim 8.5 \times 10^4$. Complete energy absorption ($\Phi = 1$) for both the packed beds occurs at Fo_d of 2.7. The uncertainty (root mean square) in energy-absorption ratio due to

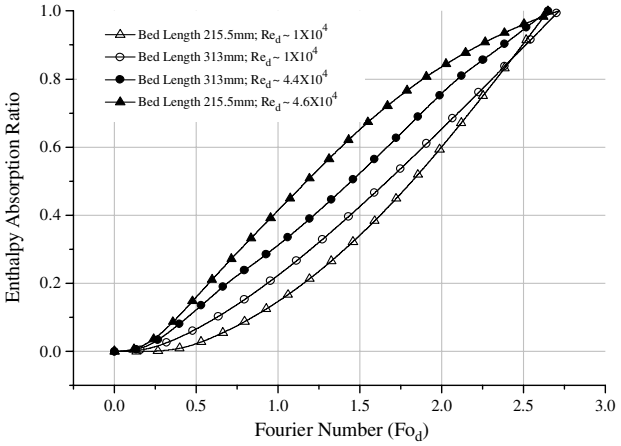

Fig. 16 Plot of energy-absorption ratio with Fourier number.

uncertainties in density, velocity, and temperature of gases (see Table 3) at 95% confidence level is 4.2%. These graphs may be used to estimate the energy absorbed (as a function of time) for geometrically similar packed beds with different packing material having thermal conductivity less than or equal to that of carbon steel ($\sim$52 W/mK), which results in Biot number being ≤ 0.1.

VII. Conclusions

The experimental study characterizes pressure drop, friction coefficients, and energy-absorption rates for packed beds at high Reynolds number range from 0.8×10^4 to 8.5×10^4. The flow temperature has no effect on the pressure drop, as can be observed from data points in Euler number plot. The longer packed bed exhibited a higher pressure drop than the shorter packed bed. With an increase in Reynolds number, the pressure drop for both the packed beds decreased and reached asymptotic values beyond Reynolds numbers of 8.5×10^4. The order of magnitude of axial conduction in the packed bed was observed to be negligible at Reynolds numbers $>10^4$. This result supports the observations of other experimenters who suggest importance of axial conduction only at low Reynolds numbers. The enthalpy absorption rate was higher for longer packed-bed length at $Re_d \sim 1 \times 10^4$ and lower at $Re_d \sim 8.5 \times 10^4$. The data presented is valid for packing of Ø9.5 mm spheres with packed-bed-to-sphere-diameter ratio of $\sim$9.5. Caution has to be exercised for usage of pressure-drop correlations and energy-absorption rate for other sphere diameters or particle shapes, even if nondimensionalized for Reynolds number. The nonapplicability, the authors feel, can be due to nonsimilar flow profiles, which along with inertia and viscous effects may result in a different pressure drop and different energy-absorption rates.

Acknowledgments

The authors would like to express their appreciations to B. S. Subash Chandran and colleagues of the Defense Research and Development Organization, Ramjet Propulsion Division along with Ground-Instrumentation Division, Hyderabad, India, for their help in setting up the experiments, data acquisition, and analysis; and to C. V. Ashok and P. Yadagiri, for fabrication and assembly and for conducting the experiments.

References

[1] Beasley, D. E. and Clark, J. A., "Transient Response of a Packed Bed for Thermal Energy Storage," *International Journal of Heat and Mass Transfer*, Vol. 27, No. 9, 1984, pp. 1659–1669. doi:10.1016/0017-9310(84)90278-3

[2] Gunn, D. J., and De Souza, J. F. C., "Heat Transfer and Axial Dispersion in Packed Beds," *Chemical Engineering Science*, Vol. 29, No. 6, 1974, pp. 1363–1371. doi:10.1016/0009-2509(74)80160-0

[3] Wakao, N., Kaguei, S., and Funazkri, T., "Effect of Fluid Dispersion Coefficients on Particle-to-Fluid Heat Transfer Coefficients in Packed Beds," *Chemical Engineering Science*, Vol. 34, No. 3, 1979, pp. 325–336.

[4] Vilemas, J. V., Margis, L. A., and Survila, V. J., "Heat Transfer from a Fixed Bed of Spheres Welded Between Two Perforated Plates," *Heat Transfer: Soviet Research*, Vol. 20, No. 4, July–Aug. 1988, pp. 533–541.

[5] Bird, R. B., Stewart, W. E., and Lightfoot, E. N., *Transport Phenomena*, Wiley, Hoboken, NJ, 2002, Chap. 6.

[6] Eisfeld, B., and Schnitzlein, K., "The Influence of Confining Walls on the Pressure Drop in Packed Beds," *Chemical Engineering Science*, Vol. 56, No. 14, 2001, pp. 4321–4329. doi:10.1016/S0009-2509(00)00533-9

[7] Gauvin, W. H., and Katta, S., "Momentum Transfer Through Packed Beds of Various Particles in the Turbulent Flow Regime," *American Institute of Chemical Engineers Journal*, Vol. 19, No. 4, July 1973, pp. 775–783. doi:10.1002/aic.690190415

[8] Glaser, M. B., and Thodos, G., "Heat and Momentum Transfer in Flow of Gases Through Packed Beds," *American Institute of Chemical Engineers Journal*, Vol. 4, No. 1, March 1958, pp. 63–74. doi:10.1002/aic.690040113

[9] Fukuda, K., Kondoh, T., and Hasegawa, S., "Similarity Rule Between Heat Transfer and Pressure Drop of Porous Media," *American Institute of Chemical Engineers Journal*, Vol. 38, No. 11, Nov. 1992, pp. 1840–1842. doi:10.1002/aic.690381115

[10] Joshi, J., and Ranade, V., "Computational Fluid Dynamics for Designing Process Equipment: Expectations, Current Status and Path Forward," *Industrial and Engineering Chemistry Research*, Vol. 42, No. 6, 2003, pp. 1115–1128. doi:10.1021/ie0206608

[11] Coussirat, M., Guardo, A., Mateos, B., and Egusquiza, E., "Performance of Stress-Transport Models in the Prediction of Particle-to-Fluid Heat Transfer in Packed Beds," *Chemical Engineering Science*, Vol. 62, No. 23, 2007, pp. 6897–6907. doi:10.1016/j.ces.2007.08.071

[12] Nijemeisland, M., and Dixon, A. G., "Comparison of CFD Simulations to Experiment for Convective Heat Transfer in a Gas-Solid Fixed Bed," *Chemical Engineering Journal*, Vol. 82 Nos. 1–3, 2001, pp. 231–246. doi:10.1016/S1385-8947(00)00360-0

[13] Kuwahara, F., Shirota, M., and Nakayama, A., "A Numerical Study of Interfacial Convective Heat Transfer Coefficient in Two Energy Equation Model for Convection in Porous Media," *International Journal of Heat and Mass Transfer*, Vol. 44, No. 6, 2001, pp. 1153–1159. doi:10.1016/S0017-9310(00)00166-6

[14] Van Der Merwe, D. F., and Gauvin, W. H., "Pressure Drag Measurements for Turbulent Air Flow Through a Packed Bed," *American Institute of Chemical Engineers Journal*, Vol. 17, No. 2, March 1971, pp. 402–409. doi:10.1002/aic.690170230

[15] International Organization for Standardization, "*Measurement of Fluid Flow by Means of Pressure Differential Devices. Part 1: General Principles and Requirements*, ISO, Geneva, 2003.

[16] Beckwith, T. G., Marangoni, R. D., and Lienhard, J. H., V, *Mechanical Measurements*, 5th ed., Pearson, Singapore, 2003, Chap. 16.

[17] Latifi, M. A., Midoux. N., and Storck, A., "The Use of Micro-Electrodes in the Study of the Flow Regimes in a Packed Bed Reactor with Single Phase Liquid Flow," *Chemical Engineering Science*, Vol. 44, No. 11, 1989, pp. 2501–2508. doi:10.1016/0009-2509(89)85194-2

[18] Jolls, K. R., and Hanratty. T. J., "Transition to Turbulence for Flow Through a Dumped Bed of Spheres," *Chemical Engineering Science*, Vol. 21, No. 12, 1966, pp. 1185–1190. doi:10.1016/0009-2509(66)85038-8

[19] Srinivasan, R., "Dimensional Analysis of Flow in Packed Beds," Advanced Systems Laboratory, Rept ASL/SPSC/2007-13, Solid Propulsion Systems Center, Defense Research and Development Organization, Hyderabad, India, 2007.

[20] Zukaukas, A., *High Performance Single-Phase Heat Exchangers*, Hemisphere, New York, 1989, Chap. 12.

[21] Winterberg, M., and Tsotsas, E., "Impact of Tube-to-Particle-Diameter Ratio on Pressure Drop in Packed Beds," *American Institute of Chemical Engineers Journal*, Vol. 46, No. 5, May 2000, pp. 1084–1088. doi:10.1002/aic.690460519

[22] Achenbach, E., "Heat and Flow Characteristics of Packed Beds," *Experimental Thermal Fluid Science*, Vol. 10, No. 1, 1995, pp. 17–27.

[23] Vortmeyer, D., and Schaefer, R. J., "Equivalence of One and Two-Phase Models for Heat Transfer Process in Packed Beds: One Dimensional Theory," *Chemical Engineering Science*, Vol. 29, No. 2, 1974, pp. 485–491.
doi:10.1016/0009-2509(74)80059-X

[24] Chan, C. K., and Tien, C. L., "Conductance of Packed Spheres in Vacuum," *Transactions of the American Society of Mechanical Engineers: Journal of Heat Transfer*, Aug. 1973, pp. 302–308.

[25] Yagi, S., Kunii, D. and Wakao, N., "Studies on Axial Effective Thermal Conductivities in Packed Beds," *American Institute of Chemical Engineers Journal*, Vol. 6, No. 4, 1960, pp. 543–546.
doi:10.1002/aic.690060407

[26] Zukauskas, A. A., and Poskas, P. S., "Effect of Velocity Fluctuations Arising in Tube Bundles in Cross Flow of Air on Coefficients of Heat Transfer at High *Re*," *Heat Transfer: Soviet Research*, Vol. 15, No. 3, May–June 1983, pp. 1–10.